ACS OMEGA

Open Access

http://pubs.acs.org/journal/acsodf

Article

Ti/Ti_4O_7 Anodes for Efficient Electrodeposition of Manganese Metal and Anode Slime Generation Reduction

Haidong Zhong, Qian Zhang,* Zuohua Liu, Jun Du, and Changyuan Tao*

Cite This: *ACS Omega* 2023, 8, 38469−38480

Read Online

ACCESS | Metrics & More | Article Recommendations | Supporting Information

ABSTRACT: Preventing lead-based anodes from causing high-energy consumption, lead pollution, and harmful anode slime emission is a major challenge for the current electrolytic manganese metal industry. In this work, a Ti_4O_7-coated titanium electrode was used as anode material (Ti/Ti_4O_7 anode) in manganese electrowinning process for the first time and compared with a lead-based anode (Pb anode). The Ti/Ti_4O_7 anode was used for galvanostatic electrolysis; the cathodic current efficiency improved by 3.22% and energy consumption decreased by 7.82%. During 8 h of electrolysis, it reduced 90.42% solution anode slime and 72.80% plate anode slime formation. Anode product characterization and electrochemical tests indicated that the Ti/Ti_4O_7 anode possesses good oxygen evolution activity, and γ-MnO_2 has a positive catalytic effect on oxygen evolution reaction (OER), which inhibited anode Mn^{2+} oxidation reaction and reduced the formation of anode slime. In addition, the low charge-transfer resistance, high diffusion resistance, and dense MnO_2 layer of the anode blocked the diffusion path of Mn^{3+} in the system and inhibited the formation of anode slime. The Ti/Ti_4O_7 anode exhibits excellent electrochemical performance, which provides a new idea for the selection of novel anodes, energy savings and emission reduction, and the establishment of a new mode of clean production in the electrolytic manganese metal industry.

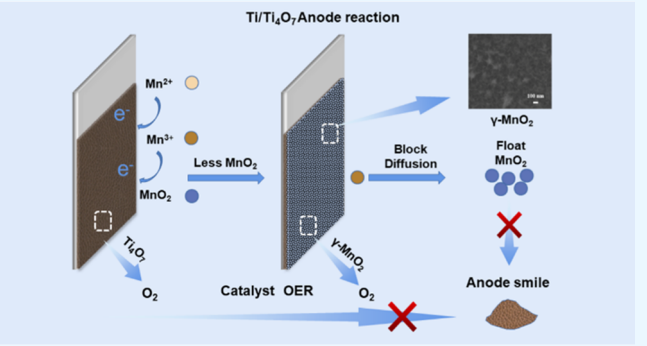

1. INTRODUCTION

Manganese is an important material. It is widely used in iron and steel smelting, nonferrous metallurgy, and new energy and other industries.[1−3] At present, metal manganese is produced by electrolysis in industry. In the process of electrodeposition of metal manganese, the electrode reactions on the cathode and anode are as follows

Cathode:

$$Mn^{2+} + 2e^- = Mn \quad E^\Theta = -1.18V \tag{1}$$

$$2H_2O + 2e^- = H_2 \uparrow + 2OH^- \quad E^\Theta = 0V \tag{2}$$

Anode:

$$2H_2O = O_2 \uparrow + 4H^+ + 4e^- \quad E^\Theta = 1.229V \tag{3}$$

$$Mn^{2+} + 2H_2O = MnO_2 \downarrow + 4H^+ + 2e^- \quad E^\Theta = 1.223V \tag{4}$$

The electroreduction of the manganese metal is the main cathodic reaction, and the side reaction is the hydrogen evolution reaction (HER). The oxygen evolution reaction (OER) is the main anodic reaction, and the side reaction is the electro-oxidation reaction to generate anode slime (mainly MnO_2). Owing to the relatively close potential of OER and MnO_2 deposition, it is difficult to avoid the side reaction of MnO_2 formation.[4] Therefore, strict control of anode slime production is one of the important technical problems and indicators for high-quality development of the electrolytic manganese industry.

In the actual production of manganese, a lead-based quaternary alloy anode (Pb−Ag−Sn-Sb) is widely used as an anode. The lead-based anode undergoes oxidation reaction in the acid system to form a smooth and dense oxide layer, which is resistant to corrosion and highly conductive, and has the stability of continuous operation.[5−7] However, the lead-based anode has a high oxygen evolution potential (OEP), which leads to the violent occurrence of anode side reactions, resulting in a large amount of anode slime.[8,9] The anode slime layer deposited on the anode surface is mainly α-MnO_2 with poor conductivity, which leads to the increase of cell voltage and energy consumption. In addition, the anode slime (MnO_2 particles) suspended in the solution can block the diaphragm and cause the short circuit of the cathode and anode.[10,11] More seriously, the lead-based anode will continue to be electro-

Received: July 21, 2023
Accepted: September 20, 2023
Published: October 9, 2023

oxidized and dissolved during the process of manganese electrowinning, and the α-MnO_2 layer is loose and porous, which cannot effectively protect the lead-based anode substrate,[12] resulting in the anode slime becoming an industrial hazardous waste containing lead.[13] At the same time, our research shows that the use of lead-based anodes in manganese electrowinning causes periodic anode potential oscillation or current oscillation, resulting in additional nonpower energy consumption, and the crystal form and morphology of the anode MnO_2 layer are the main factors inducing electrochemical oscillation.[14,15] Therefore, exploring a novel anode instead of a lead-based anode can reduce the production of anode slime and lead pollution and improve current efficiency in manganese electrowinning, which plays an important role in promoting the clean production and sustainable development of the electrolytic manganese industry.

Coated titanium anode is a promising novel anode for manganese electrodeposition, which can replace the lead-based anode.[16] Liu et al. investigated the performance of the Ti/IrO_2−RuO_2−SiO_2 anode for manganese electrowinning in an anion-exchange membrane electrolysis reactor; the current efficiency increased by 10% while energy consumption decreased by 27%, and no anode slime was produced.[17] Luo et al. prepared a Ti/$Ru_{1/3}Sn_{2/3}O_2$ anode, which exhibited excellent OER catalytic performance and reduced about one-third of the anode slime.[18] Coated titanium anodes still have disadvantages of a complex preparation process, participation of precious metals, and difficulty in maintaining coating activity. Therefore, coating materials with low cost, high coating catalytic activity, and stability become necessary. As a member of the Magnéli phase (Ti_nO_{2n-1}, $n \geq 4$), Ti_4O_7 has the advantages of good electrical conductivity, excellent chemical stability in acidic systems, and strong cost competitiveness.[19,20] Li et al. used a Ti_4O_7 anode to electro-oxidate tetracycline (TC) in wastewater, and the total removal rate of TC was more than 90%.[21] The S/Ti_4O_7 composite cathode prepared by Liu et al. exhibited a capacity decay of about 0.09% per cycle in 500 cycles and low battery-transfer resistance.[22] Li et al. studied the performance of the electrode with Ti_4O_7 material and found that the electrode has both oxygen reduction reaction and OER activity.[23] Han et al. studied the performance of the Al/Ti_4O_7/RuO_2−TiO_2−SnO_2 anode and found that the electrode potential was evenly distributed. The current efficiency and electrolysis energy consumption were 5.59% higher and 16.2% lower than theTi/RuO_2−TiO_2 anode in cobalt electrodeposition, respectively.[24] Although Ti_4O_7 has shown technical applications in environmental water treatment, fuel cells, and batteries,[22,25,26] the application of Ti_4O_7-coated anodes in manganese electrodeposition has not been studied.

In this study, a Ti_4O_7-coated titanium anode (Ti/Ti_4O_7 anode) was applied to manganese electrodeposition for the first time. The anode performance, anode reaction, and anode slime formation mechanism of the Ti/Ti_4O_7 anode were investigated, and the lead-based anode (Pb anode) was used as the comparison electrode. The feasibility of the Ti/Ti_4O_7 anode as an alternative anode material for industrial manganese electrodeposition was evaluated by a galvanostatic electrolysis experiment. The chemical composition and microstructure of anode products were characterized by scanning electron microscopy (SEM), X-ray photoelectron spectroscopy (XPS), and X-ray diffraction (XRD). The anodic reaction mechanism of the Ti/Ti_4O_7 anode in the process of electrodeposition of manganese was further clarified by electrochemical tests such as cyclic voltammetry (CV), linear voltammetry (LSV), chronopotentiometry (CP), Tafel polarization test, and electrochemical impedance spectroscopy (EIS). This study aims to provide a theoretical basis for the electrolytic manganese metal industry to find alternative, energy-saving, and environmentally friendly anode materials.

2. EXPERIMENTAL SECTION

2.1. Materials. The Ti/Ti_4O_7 anode was kindly supplied by Changsha Purong Chemical Co., Ltd. The Ti/Ti_4O_7 anode was prepared by the plasma spraying method, the preparation method (Text S1) is discussed in the Supporting Information. The lead-based quaternary alloy anode ($PbSb_{0.003}Sn_{0.0003}Ag_{0.0003}$) was provided by Southern Manganese Group Co., Ltd. Manganese sulfate ($MnSO_4{\cdot}H_2O$), ammonium sulfate ($(NH_4)_2SO_4$), selenium dioxide (SeO_2), and sulfuric acid (H_2SO_4) were all analytical grade, purchased from Guoyao Holding Chemical Reagents Co., Ltd. All reagents were prepared by using ultrapure water (specific resistance of 18 MΩ·cm). The composition of the simulated manganese sulfate electrolyte is 30 g L^{-1} Mn^{2+} ($MnSO_4$), 120 g L^{-1} $(NH_4)_2SO_4$, and 30 mg L^{-1} SeO_2.

2.2. Electrochemical Measurement. Electrochemical analysis was carried out using an electrochemistry workstation (CHI660E, Shanghai Chenhua) with a three-electrode system. Ti/Ti_4O_7 and Pb anodes with a working area of 1 cm^2 were used as working electrodes, and a stainless steel electrode and a saturated calomel electrode (SCE) were used as counter electrode and reference electrode, respectively. When the cathodic current density is 350 A m^{-2}, the change of anode potential with time under direct current (DC) power and hyperchaotic circuit (HCC) was tested by CP. In the electrolyte without Mn^{2+} (120 g L^{-1} $(NH_4)_2SO_4$, 30 mg L^{-1} SeO_2), the LSV test was carried out at a scanning rate of 10 mV s^{-1}. The polarization curve was plotted by the relationship between the overpotential (η) and log (j). In the $MnSO_4$ electrolyte, the EIS test was performed at an open circuit voltage with an amplitude of 5 mV and a frequency range of 0.01 Hz to 100 kHz. CV tests were performed at a scan rate of 5 mV s^{-1} in the potential range of 0.3−2.0 V and 5, 10, 15, 25, and 50 mV s^{-1} in the potential range of 0.3−1.8 V. The Tafel polarization test was performed at a scan rate of 10 mV s^{-1} in a 1 mol/L H_2SO_4 solution, and the test range was from 0 to 1.2 V.

2.3. Characterization Techniques. The morphology of the anode and anode slime were characterized by SEM (VEGA IILMA, TESCAN). The phase and elemental compositions of Ti_4O_7 coating and plate anode slime were determined by XRD (D/Max-2500, j Rigaku) using Cu Kα radiation. The chemical composition and elemental valence were analyzed by XPS (ESCALAB250Xi, Thermo Scientific). The binding energy values were corrected using the carbon C 1s binding energy at 284.8 eV.

2.4. Electrolysis Experiments. Galvanostatic electrolysis was conducted in 450 mL of laboratory cell electrolyte solution capacity. The anode area and cathode area are separated by a nonwoven membrane. The anode was a flat Ti/Ti_4O_7 anode or a Pb anode (3.0 × 4.5 cm^2 per piece), and the cathode was a stainless steel sheet (3.0 × 4.5 cm^2 per piece). The cathode current density of 350 A m^{-2} was maintained by a DC-regulated power supply for electrolysis, and the electrolysis time was set to 2, 4, 6, and 8 h. During long-term electrolysis

https://doi.org/10.1021/acsomega.3c05273
ACS Omega 2023, 8, 38469−38480

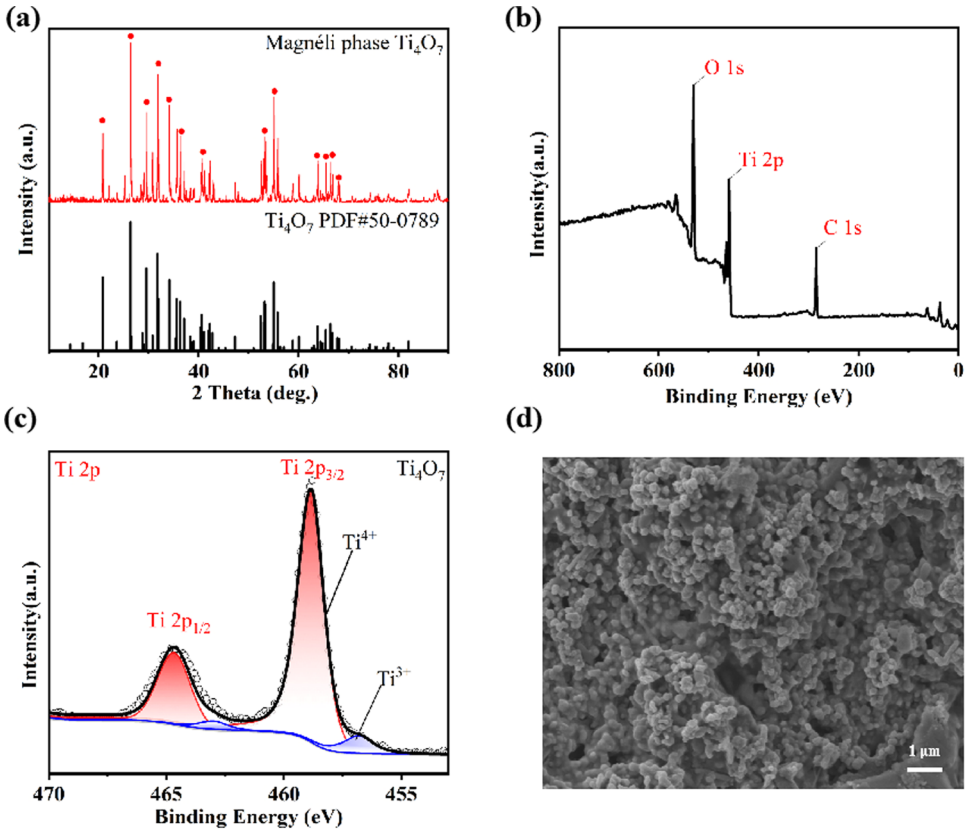

Figure 1. Characterization of the Ti/Ti_4O_7 anode: (a) XRD spectrum of the Ti_4O_7 powder, (b) XPS full spectrum of the Ti_4O_7 powder, (c) Ti 2p, and (d) SEM image of the anode surface.

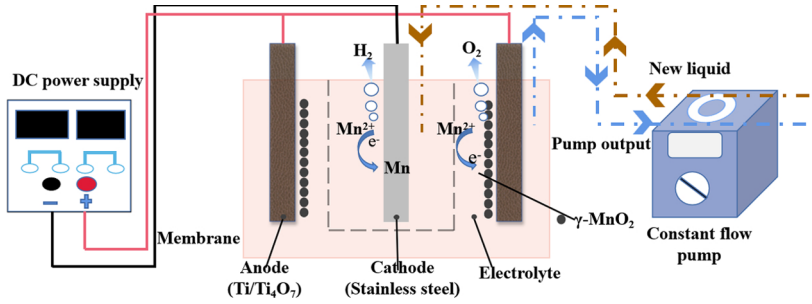

Figure 2. Schematic diagram of the manganese electrolysis experiment using the Ti/Ti_4O_7 anode.

(after 2 h), the electrolyte was supplemented and extracted by a circulating pump. The cathode current efficiency (CE) and the energy consumption (EC) for Mn electrowinning were calculated as follows

$$CE = \Delta m/(q \cdot i \cdot \Delta t) \quad (5)$$

$$EC = (U \cdot 1000)/(q \cdot CE) \quad (6)$$

where $\Delta m/\Delta t$ is the mass gain per unit area of the cathode over the time interval Δt (g h^{-1}); i is the applied current (A); q is the electrochemical equivalent of Mn (1.025 g (A h)$^{-1}$); EC is the energy consumption ((kW h) t^{-1}); and U is the cell voltage (V).

3. RESULTS AND DISCUSSION

3.1. Chemical Composition and Structural Characteristics. Figure 1a shows the XRD pattern of the Ti_4O_7 powder in the coating material. The major peaks matching the characteristic peaks of Ti_4O_7 (PDF card 50−0789) occur at 20.7, 26.3, 31.7, 34.0, 40.5, 53.1, 55.0, 66.4, and 67.8° (and indicated by red dots), confirming the presence of the Magnéli phase Ti_4O_7 as the major composition. Ti_5O_9 also exists (Figure S1); Ti_4O_7 and Ti_5O_9 are the most conductive titanium oxides, which do not affect the conductivity of the electrode.[27,28] XPS was employed to identify the chemical composition and element combination state of the Ti_4O_7 powder. The XPS full spectrum shown in Figure 1b confirms the coexistence of Ti and O elements. Figure 1c shows the Ti 2p double peak of Ti_4O_7. Ti $2p_{3/2}$ has a tail at 456.8 eV, which is a typical feature of Ti^{3+}, and the main peak at 459.0 eV can be assigned to Ti^{4+}.[20] According to the XPS spectrum, there is about 18% Ti^{3+} in the structure of the Magnéli phase Ti_4O_7. The valence state of the Ti_4O_7 powder in the coating is consistent with the results of Tominaka et al., indicating that the crystal structure of Ti_4O_7 is rutile block interspersed with corundum-like Ti_2O_3 layer, and the resulting vacancies may

https://doi.org/10.1021/acsomega.3c05273
ACS Omega 2023, 8, 38469−38480

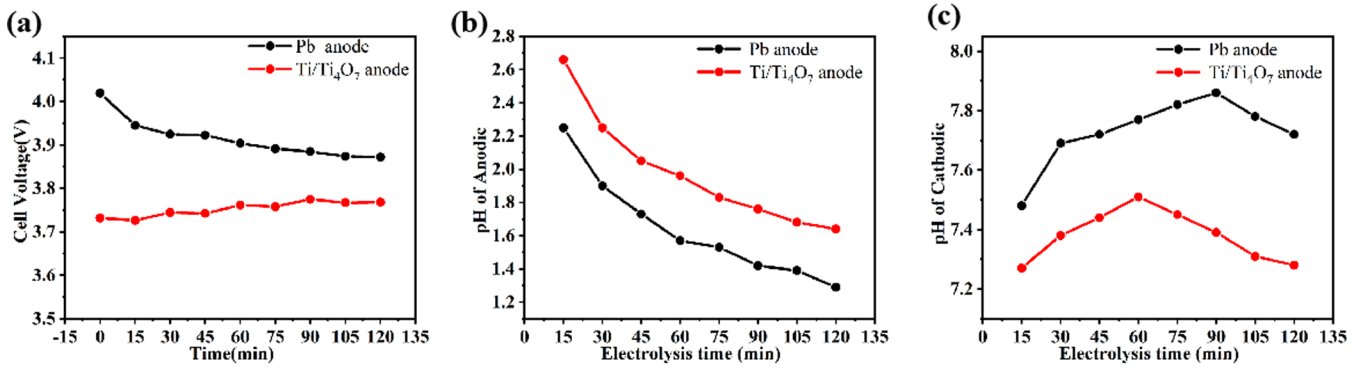

Figure 3. Experimental parameters of electrolysis process: (a) cell voltage, (b) pH of the anodic solution, and (c) pH of the cathodic solution.

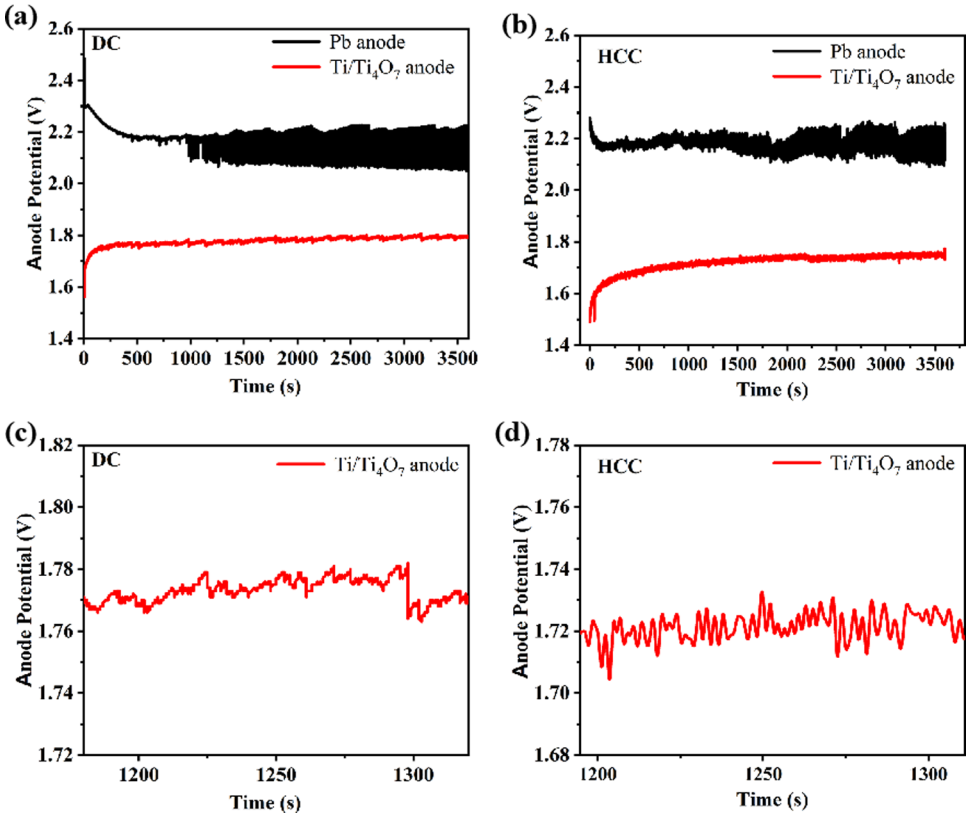

Figure 4. Anodic potential−time curves of galvanostatic polarization for 1 h under different power sources: (a, c) DC and enlarged view; (b, d) HCC and enlarged view.

allow sufficient shrinkage in the lattice, resulting in high conductivity of the Magnéli phase titanium oxide.[29] The SEM of the anode surface shown in Figure 1d, and the microstructure of the Ti/Ti_4O_7 anode surface, presents a dense honeycomb-like surface. The Ti_4O_7 aggregates are tightly packed in spherical particles with a particle diameter of 60−100 nm. There are abundant porous channels on the anode surface, which provide sufficient surface area and internal space to expose more reactive sites.

3.2. Experimental Study on Electrolysis Process. The galvanostatic electrolysis for 2 h was carried out at a cathode current density of 350 A m^{-2} to evaluate the feasibility of the Ti/Ti_4O_7 anode as an alternative anode material for industrial manganese electrodeposition. The schematic diagram of the electrolysis experiment is shown in Figure 2, and the Pb anode serves as the comparison anode. As presented in Figure 3a, the U of the Pb anode decreased from 4.02 to 3.87 V after 2 h. For the Ti/Ti_4O_7 anode, the U increased with the electrolysis, from 3.73 to 3.77 V. This is because MnO_2 gradually covers the surface of the Ti/Ti_4O_7 anode, and the OER process is transferred to the MnO_2 layer, resulting in different changes. The average cell voltages (U_{aver}) of Ti/Ti_4O_7 and Pb anodes were 3.752 and 3.915 V, respectively, which decreased by about 163 mV. The CE was 83.80%, which was 3.22% higher than that of the Pb anode, and EC was 4368.12 k Wh t^{-1}, reduced by 7.82%, which shows excellent anode performance. In Figure 3b, the pH of the anode region decreases with the increase of time. The average pH values of the Ti/Ti_4O_7 anode and the Pb anode were 1.98 and 1.63, respectively. The Ti/Ti_4O_7 anode has a higher pH, indicating that the solution becomes acidic and can inhibit the hydrolysis reaction of Mn^{3+} in the solution to form anode slime.[30] The pH of the cathode

https://doi.org/10.1021/acsomega.3c05273
ACS Omega 2023, 8, 38469−38480

region showed a trend of increasing first and then decreasing (Figure 3c). This is because the hydrogen evolution overpotential of the Mn metal is higher than that of the stainless steel.[31] Under the Ti/Ti_4O_7 anode, the cathode pH is lower and the maximum pH value appears 30 min earlier. The possible reasons could be explained as Mn is uniformly covered on the cathode earlier and the HER is inhibited.[32]

The anode potential was analyzed under DC and HCC. The design and principle of the hyperchaotic circuit have been shown in a previous research work.[33] The anode potential−time curves under the HCC before filtering are shown in Figure S2. As presented in Figure 4a,b, the Pb anode has an obvious electrochemical oscillation phenomenon, resulting in additional energy consumption. Under the Ti/Ti_4O_7 anode, there was no obvious anodic electrochemical oscillation, but only a slight fluctuation of the anode potential (Figure 4c,d). In DC polarization, the anode potential of the Ti/Ti_4O_7 anode and Pb anode was 1.8 and 2.23 V, respectively, and the average anode potential of the Ti/Ti_4O_7 anode was 430 mV lower. In HCC polarization, the anode potential was 1.75 and 2.19 V, respectively, and the Ti/Ti_4O_7 anode still has low anode potential. The application under different power sources showed that the anode potential under the Ti/Ti_4O_7 anode was reduced, which greatly reduced the energy consumption of electrolysis and avoided the additional energy consumption caused by the electrochemical oscillation.

The stability of the Ti/Ti_4O_7 anode and the distribution of anode slime were investigated, and long-term electrolysis experiments (2, 4, 6, 8 h) were carried out. The experimental parameters of the electrolysis process are given in Table 1. The

Table 1. Ti/Ti_4O_7-Anode Galvanostatic Electrolysis Experimental Results

	U_{aver} (V)		CE (%)		EC (kwh t^{-1})	
experiment time(h)	Pb	Ti_4O_7	Pb	Ti_4O_7	Pb	Ti_4O_7
2	3.85	3.71	80.84	82.97	4646.33	4362.43
4	3.91	3.82	79.77	81.95	4782.04	4547.68
6	3.88	3.76	80.74	82.6	4688.34	4441.03
8	3.84	3.74	77.58	80.04	4829.04	4558.71

U_{aver} of the Ti/Ti_4O_7 anode in 2−8 h was 3.71, 3.82, 3.76, and 3.74 V, respectively, which was 100−150 mV lower than that of Pb anode at the same time. After 8 h of electrolysis, compared with the Pb anode, CE of the Ti/Ti_4O_7 anode improved by 2.48% and EC reduced by 5.60%.

The anode slime on the plate and that suspended in the solution were collected, cleaned, and dried, respectively. The formation and composition of different positions are shown in Figure 5. Under the Pb anode, red-brown anode slime was rapidly formed in the electrolyte; after a period of time, MnO_2 covered the surface of the anode, and a large number of black particles were suspended in the electrolyte. Under the Ti/Ti_4O_7 anode, the anode product was mainly produced on the anode and the solution is always kept in a transparent state. After 8 h of electrolysis, the solution anode slime was 0.0748 g, which was reduced 90.42%. The plate anode slime was 0.3273 g, which was reduced 72.80%. In summary, the Ti/Ti_4O_7 anode has the function of stable and efficient operation for a long time inhibiting the formation of anode slime.

3.3. Chemical Composition and Morphology Analysis of Anode Slime. In order to explore the mechanism of anode slime generation under the Ti/Ti_4O_7 anode, the plate anode slime was collected, and the phase, composition, and surface morphology were analyzed. The XRD spectra of the plate anode slime under different anodes are shown in Figure 6.

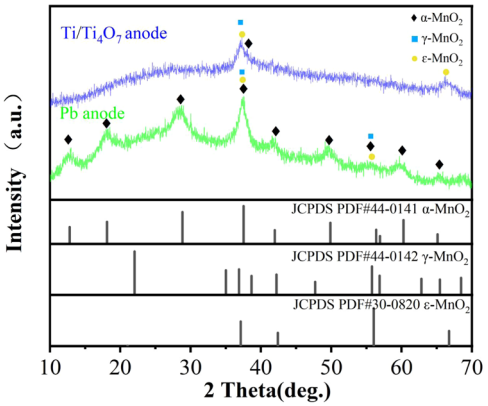

Figure 6. XRD patterns of the plate anode slime under different anodes.

MnO_2 produced under the Pb anode and the Ti/Ti_4O_7 anode contained α-MnO_2, γ-MnO_2, and ε-MnO_2, but there were some differences. For the Pb anode, the peaks at 12.5, 18.0, 28.3, 37.5, 41.9, 55, and 65.4° were indexed to the characteristic peaks of the α-MnO_2 phase (PDF card 44−

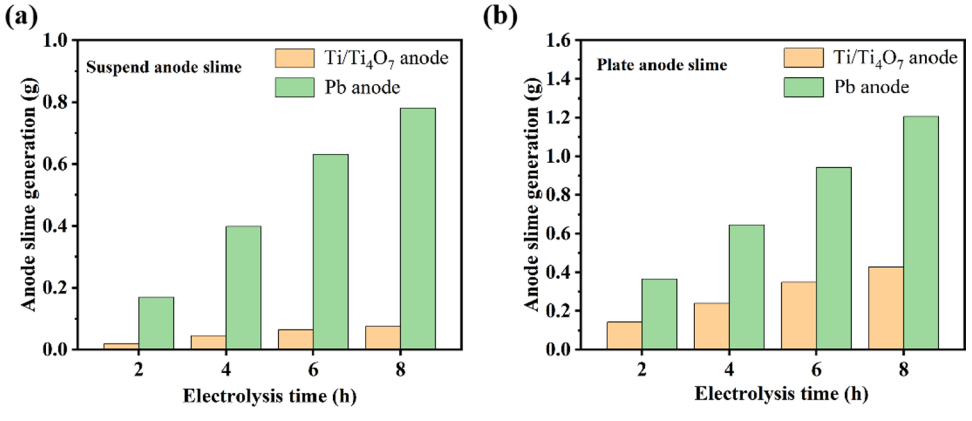

Figure 5. Generation and distribution of anode slime under different anodes: (a) solution anode slime and (b) plate anode slime.

https://doi.org/10.1021/acsomega.3c05273
ACS Omega 2023, 8, 38469−38480

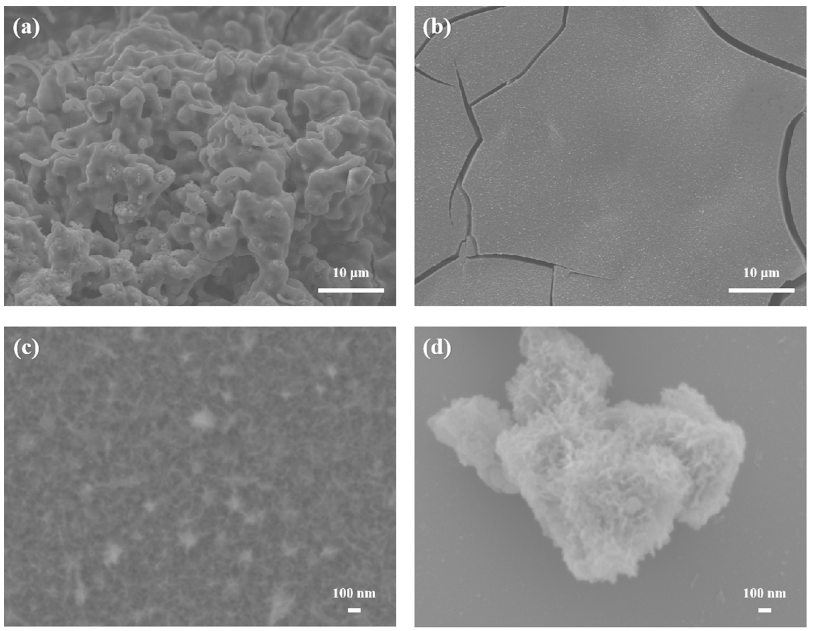

Figure 7. SEM images of anode slime under different anodes: (a) Pb anode MnO_2 layer, (b) Ti/Ti_4O_7 anode MnO_2 layer, (c) the enlarged view of the MnO_2 layer on the Ti/Ti_4O_7 anode, and (d) Ti/Ti_4O_7 anode slime.

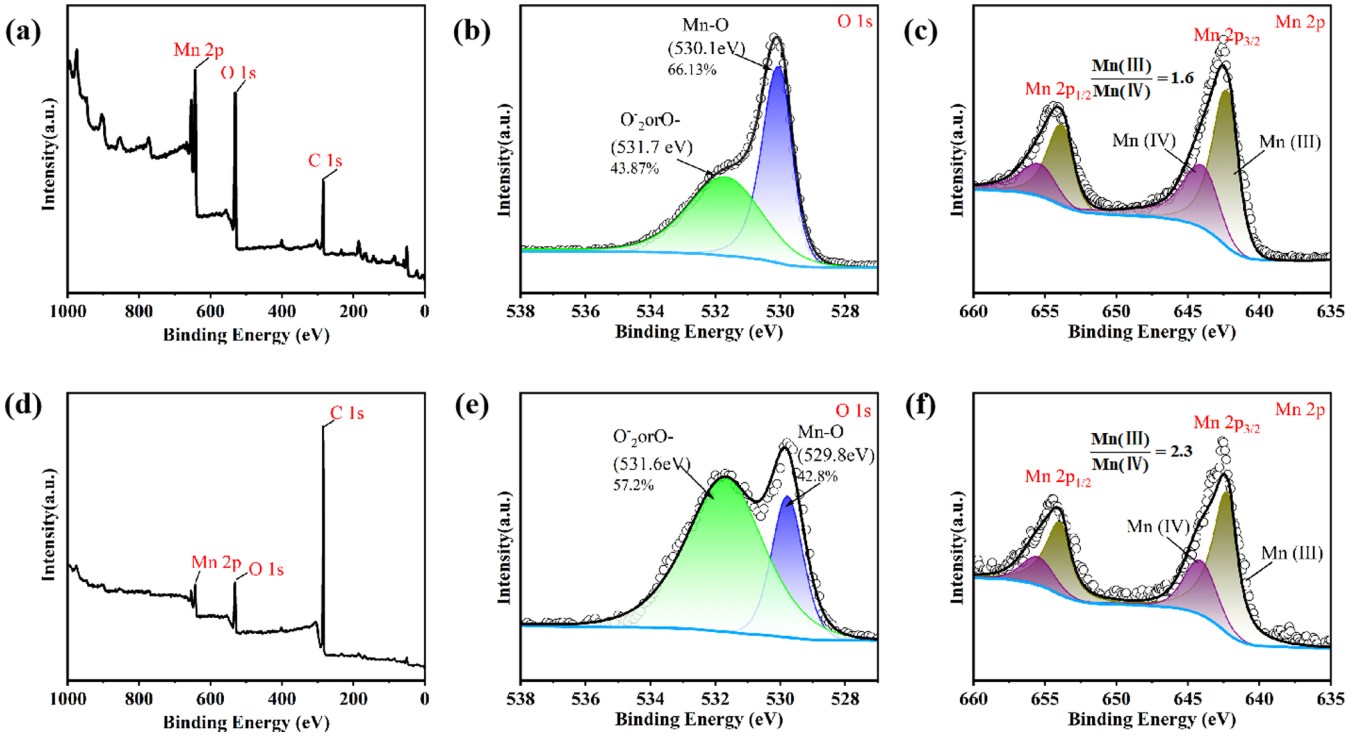

Figure 8. XPS spectra of anode slime: (a–c) Pb anode, (d–f) Ti/Ti_4O_7 anode, (a, d) full spectrum, (b, e) O 1s, and (c, f) Mn 2p.

0141). The XRD pattern of the deposits on the Ti/Ti_4O_7 anode has prominent diffraction peaks at 37.1 and 66.3°. The MnO_2 layer electrodeposited on the Ti/Ti_4O_7 anode is a combination of γ-MnO_2 and ε-MnO_2 (mainly γ-MnO_2). As known, the gamma (γ) and akhtenskite (ε) polymorphs are often considered as the most active phase for aqueous reaction.[34]

The microstructure of the MnO_2 layer on the Pb anode is shown in Figure 7a, and a rough and porous surface and fluffy accumulation of the manganese oxide layer were observed. This led to lead contamination and the occurrence of hydrolysis sludge, which would affect the purity of the electrolytic product.[9] For the microstructure of the MnO_2 layer on the Ti/Ti_4O_7 anode (Figure 7b), the surface of MnO_2 was smooth and dense, which uniformly covered the surface of the anode. This physically isolated the Ti/Ti_4O_7 substrate from the electrolyte and effectively improved the corrosion resistance of the anode coating. Interestingly, needle-like γ-MnO_2 (Figure 7c,d) was found in the local amplification diagram and anode slime particles, respectively, confirming the

https://doi.org/10.1021/acsomega.3c05273
ACS Omega 2023, 8, 38469−38480

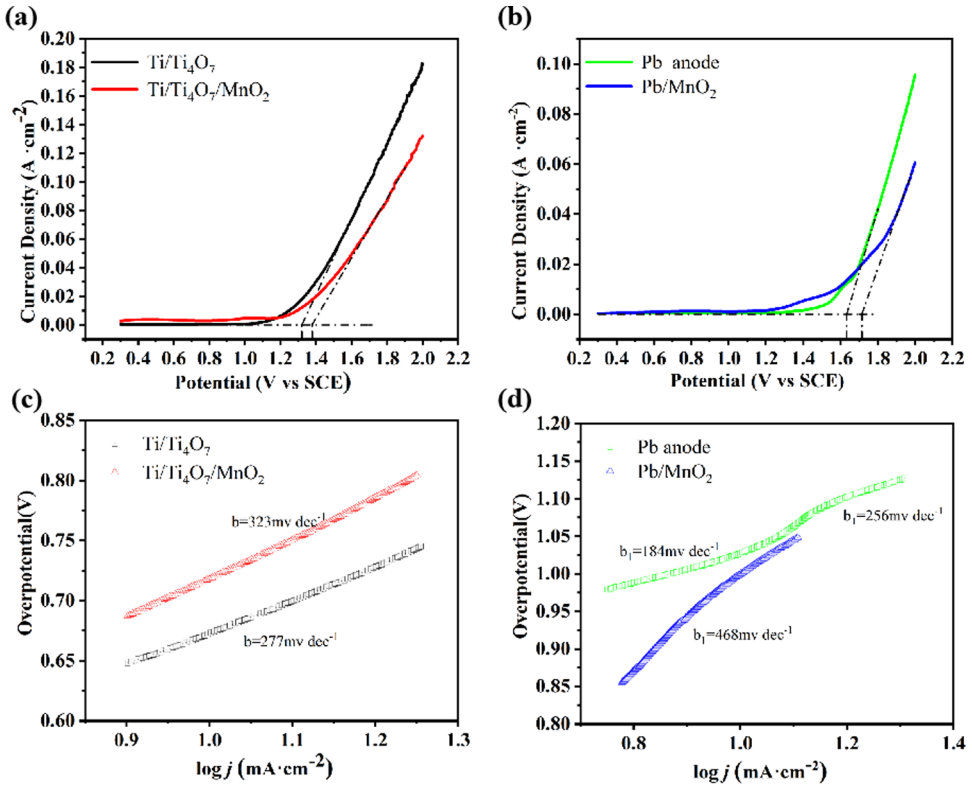

Figure 9. LSV curves for the OER at a scan rate of 5 mV s^{-1}: (a, b) Ti/Ti_4O_7 anode and Pb anode, (c, d) LSV curve corresponding Tafel plots.

XRD results. The needle-like γ-MnO_2 increased the specific surface area of the anode, reduced the cell pressure, and has better oxygen evolution performance.[35,36] γ-MnO_2 has excellent oxygen evolution performance, as tested below. Meanwhile, this explains the maintenance of oxygen evolution activity and the decrease of anode potential of the Ti/Ti_4O_7 anode during electrolysis. The morphology of anode sediment particles under different anodes can be seen (Figure S3), and the morphology of the anode mud particles is consistent with the surface MnO_2 layer.

XPS analysis was performed to characterize the surface elemental composition and the chemical valence of the plate anode slime, and all peaks were calibrated at the peak position of C 1s. The full spectrum in Figure 8a,d shows that the anode slime under the two anodes was composed of Mn, O, and C elements. The O 1s spectrum of anode slime under the Ti/Ti_4O_7 anode was located at 530.10 and 531.70 eV (Figure 8b), and anode slime under the Pb anode was located at 529.80 and 531.60 eV (Figure 8e). The main peak with a binding energy of about 530 eV represented metal oxides, while the peak with a binding energy of about 531.60 eV may be chemisorption oxygen such as low-coordinated O^{2-} or O^-.[37,38] The XPS spectra of Mn 2p in Ti/Ti_4O_7 anode slime after electrolysis are shown in Figure 8c. The Mn $2p_{3/2}$ binding energy peak was located at 642.3 eV, and the $2p_{1/2}$ peak was located at 654.0 eV. The peak position distance between Mn $2p_{3/2}$ and $2p_{1/2}$ was 11.7 eV, which was in good agreement with the reported data of MnO_2.[4,39] The main peak of binding energy at 642.3 eV was ascribed to Mn (III), and the binding energy at 644.0 eV was attributed to Mn (IV).[40,41] There was a significant difference in the valence state of manganese in the anode slime under the electrolysis of the Pb anode and the Ti/Ti_4O_7 anode. The relative content ratio of Mn(III) and Mn(IV) in deposited MnO_2 is shown in Table S1. The ratio of Mn (III) to Mn (IV) in the anode slime under the Ti/Ti_4O_7 anode was 2.3, and that under the Pb anode was 1.6. The rich Mn (III) in the lattice is responsible for the superior OER performances.[42]

Through the above analysis of the surface morphology, chemical composition, and element valence of anode slime under different anodes, the variability in the formation mechanism of anode slime is investigated. The anode slime of the Pb anode was mainly α-MnO_2 crystal, which limited its catalytic oxygen evolution performance, resulting in a large amount of anode slime and a loose MnO_2 layer.[4] Variation in anode slime formation under different anodes can be explained by the hydrolysis mechanism of Mn^{2+} oxidation, which is given by eqs 7–9.[30,43] In summary, the Ti_4O_7 coating has high conductivity, which provided a large number of reactive sites, and generated a uniform and dense γ-MnO_2 layer. Needle-like γ-MnO_2 has higher catalytic oxygen evolution activity and conductivity, which inhibited the oxidation of Mn^{2+} (eq 7) and reduced the formation of anode slime. Dense MnO_2 layer and higher pH anode solution during the electrolysis process relatively completely inhibited the diffusion of Mn^{3+} into the solution to produce solution anode slime (eqs 8, 9).

$$Mn^{2+} = Mn^{3+} + e^- \quad (7)$$

$$Mn^{3+} + 2H_2O = MnOOH + 3H^+(fast) \quad (8)$$

$$MnOOH = MnO_2 + H^+ + e^-(slow) \quad (9)$$

3.4. Analysis of Anodic Reaction Mechanism. The OER activity of the Ti/Ti_4O_7 anode and the deposited MnO_2 layer were evaluated in a simulated electrolyte without Mn^{2+}. Figure 9a,b shows the LSV polarization curves of the two anodes at a scan rate of 5 mV s^{-1}. The initial OEP of the corresponding anode can be obtained by tangenting the stable

https://doi.org/10.1021/acsomega.3c05273
ACS Omega 2023, 8, 38469−38480

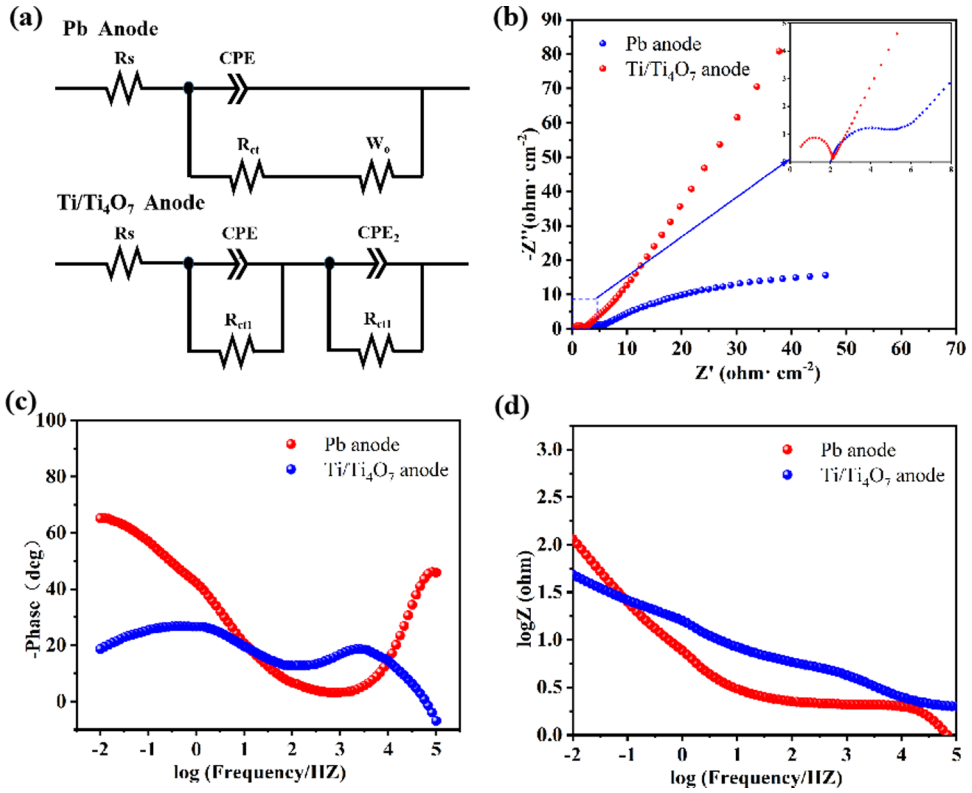

Figure 10. EIS with the Ti/Ti_4O_7 and Pb anodes: (a) Nyquist plots, (b) equivalent circuit model of the anodes, and (c, d) Bode plots of the anodes.

Table 2. Electrochemical Data and the Corresponding Relative Errors Determined from EIS Plots with a Pb Anode

R_s ($\Omega \cdot cm^{-2}$)	CPE_1 ($F \cdot cm^{-2}$)	R_{ct1} ($\Omega \cdot cm^{-2}$)	CPE_2 ($F \cdot cm^{-2}$)	R_{ct2} ($\Omega \cdot cm^{-2}$)
1.98 (1.24%)	5.98×10^{-4} (4.5%)	2.71 (4.24%)	3.76×10^{-2} (1.45%)	73.98 (5.43%)

oxygen evolution stage. For the Ti/Ti_4O_7 and Pb anodes, the OEP values were 1.319 and 1.633 V, respectively, 324 mV lower than that of the Pb anode. After deposition of the MnO_2 layer, the initial OEP of the Ti/Ti_4O_7 anode was 335 mV lower than that of the Pb anode. On the basis of the LSV, the corresponding Tafel plots of the two anodes were determined (Figure 9c,d). For the Pb anode, the Tafel plots have a double slope behavior in the low potential region and the high potential region; with the increase of potential, the OER becomes the dominant reaction.[44,45] For the polarized Pb anode, the Tafel slope of the OER process was 468 mV dec^{-1}, and for the polarized Ti/Ti_4O_7 anode, the Tafel slope was 323 mV dec^{-1}, which shows the kinetic advantages of the Ti/Ti_4O_7 anode in the OER process. In manganese electrowinning, the Ti/Ti_4O_7 anode always maintains good oxygen evolution activity, which can reversely inhibit the manganese oxidation reaction, thereby reducing the plate anode slime.

EIS measurements were conducted to analyze the electron-transfer characteristics and anodic reaction of the Ti/Ti_4O_7 anode. The equivalent circuit model obtained by EIS and the corresponding Nyquist diagram are shown in Figure 10. The data were simulated according to the Equivalent Circuit (Figure 10a), where R_s is the solution resistance, R_{ct} is the charge-transfer resistance, W_0 is the Warburg diffusion resistance, and CPE_1 is the double-layer capacitance. For the Pb anode, two capacitor rings were observed in the Nyquist plots (Figure 10b), and the Bode plot showed two time constants (Figure 10c). This indicates that the reaction process was composed of two charge-transfer control processes. For the Ti/Ti_4O_7 anode, the anodic reaction characteristics changed significantly. A semicircle appeared in the high frequency region of the Nyquist plots, indicating that the charge-transfer step was likely the control step; the linear correlation in the low frequency region indicates that the anodic reaction process was diffusion-controlled.[46,47]

Data were simulated according to the model circuit shown in Tables 2 and 3. Anode electrode reaction R_{ct} was reduced from

Table 3. Electrochemical Data and the Corresponding Relative Errors Determined from EIS with a Ti/Ti_4O_7 Anode

R_s ($\Omega \cdot cm^{-2}$)	CPE ($F \cdot cm^{-2}$)	R_{ct} ($\Omega \cdot cm^{-2}$)	Z_w ($\Omega \cdot cm^{-2}$)
1.94 (1.51%)	3.85×10^{-6} (3.02%)	1.81 (1.21%)	470.3 (1.35%)

73.98 $\Omega\ cm^{-2}$ of the Pb anode to 1.81 $\Omega\ cm^{-2}$. The Ti/Ti_4O_7 anode has a low charge-transfer resistance. W_0 is 470.3 $\Omega\ cm^{-2}$, indicating that the diffusion of ions in the solution was the limiting step of the anodic reaction.[48] After the Ti/Ti_4O_7 anode was used, the control step of the anodic reaction changed from a charge-transfer process to a charge-transfer process and a diffusion process. Combined with the analysis of the Ti/Ti_4O_7 anode surface morphology, the honeycomb Ti_4O_7 particle clusters on the anode surface have good electron transport properties, providing a larger interface area and a large number of reactive sites for the anodic electrochemical

https://doi.org/10.1021/acsomega.3c05273
ACS Omega 2023, 8, 38469−38480

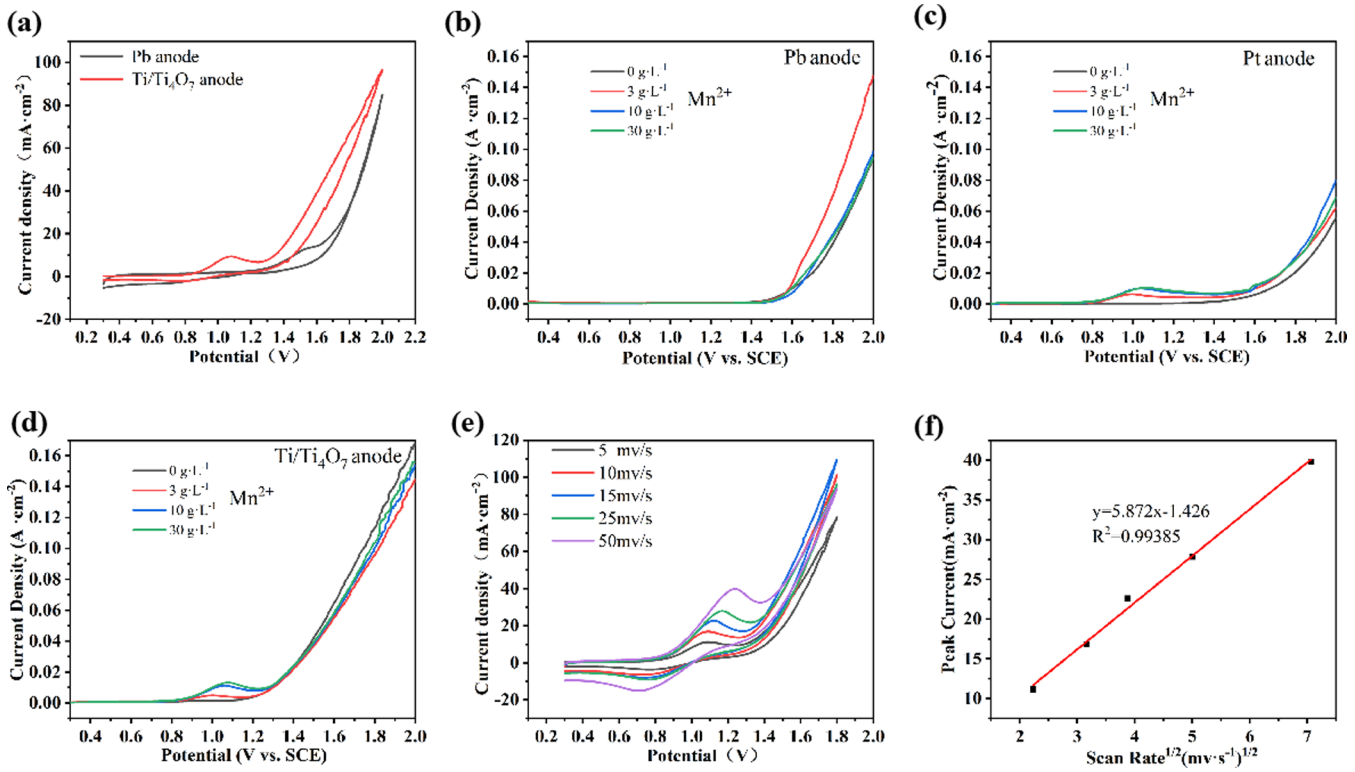

Figure 11. Ti/Ti_4O_7 anode reaction electrochemical test: (a) CV curve with a Pb anode in the $MnSO_4$ electrolyte, (b−d) LSV curves of the Pb, Pt, and Ti/Ti_4O_7 anodes in different Mn^{2+} concentrations in the electrolyte, (e) CV curves of the Ti/Ti_4O_7 anode at different potential scanning rates (5, 10, 15, 25, and 50 mV/s), and (f) relationship between the anodic oxidation peak current and the potential scanning rate of the Ti/Ti_4O_7 anode.

Table 4. Corrosion Performance Parameters in Tafel Curves of the Ti/Ti_4O_7 and Pb Anodes under Different Polarization Times

anode	Pb anode			Ti/Ti_4O_7 anode		
time (min)	$j_{corr}\times10^{-4}$ (A·cm^{-2})	E_{corr} (V)	R_p (Ω)	$j_{corr}\times10^{-4}$ (A·cm^{-2})	E_{corr} (V)	R_p (Ω)
0	1.694	−0.378	258.1	0.359	−0.650	607.9
5	1.986	0.162	165.1	1.025	0.590	328
15	2.738	0.255	149.2	1.181	0.627	320.4
30	3.085	0.287	131.6	3.046	0.648	127.7
50	4.517	0.334	97.4	2.764	0.652	164.4
60	4.007	0.441	108.3	2.254	0.656	171.4

reaction.[49,50] This makes the Ti/Ti_4O_7 anode exhibit excellent charge-transfer performance, and Mn^{2+} can be rapidly and thoroughly oxidized at the interface to form a uniform and dense active γ-MnO_2 layer. The high diffusion resistance also blocks the diffusion path of Mn^{3+} in the system.

The anodic reaction mechanism of the Ti/Ti_4O_7 anode was investigated. CV test was carried out in the $MnSO_4$ electrolyte at a scanning rate of 5 mV s^{-1}. As shown in Figure 11a, the CV curve of the Pb anode does not show the redox peak of manganese, and the lead oxidation peak appears at 1.5 V. The CV curve of the Ti/Ti_4O_7 anode shows a pair of redox peaks. The oxidation peak is at about 1.1 V, and the reduction peak is nearly 0.8 V. However, the peak current of the reverse reduction peak is small, which shows that partial reversible reaction of manganese may occur in the anode.[51] In order to determine whether the oxidation peak in the CV curve is caused by the oxidation of manganese, an LSV test of the anode at different Mn^{2+} concentrations was carried out. A Pb anode and a platinum electrode (Pt anode) were selected as the comparison anode. Only the oxidation peak and oxygen evolution characteristic curve of lead appeared on the Pb anode (Figure 11b). The oxidation peak of the Pt anode appeared at about 1.1 V, and the peak current increased with the increase of Mn^{2+} concentration (Figure 11c). The Ti/Ti_4O_7 electrode also has an oxidation peak at 1.1 V, and the change in trend of the peak current density is the same as that of the Pt anode (Figure 11d). Through the comparison experiments, it could be obtained that the anodic peak on the Ti/Ti_4O_7 anode at about 1.1 V is the oxidation reaction of Mn^{2+}. Combined with CV test, it shows that the oxidation effect of Mn^{2+} on the Ti/Ti_4O_7 anode is more significant than that on the Pb anode. The oxidation reaction is faster, and the anode surface is faster to generate a dense MnO_2 layer. Figure 11e shows the CV curves of the Ti/Ti_4O_7 anode at different scan rates in the range of 5−50 mV s^{-1}. The shape of the CV curve is not affected by the change of the potential scanning rate. The redox potential difference enlarges with the increases of the scanning speed, and all of them show symmetrical partial

https://doi.org/10.1021/acsomega.3c05273
ACS Omega 2023, 8, 38469−38480

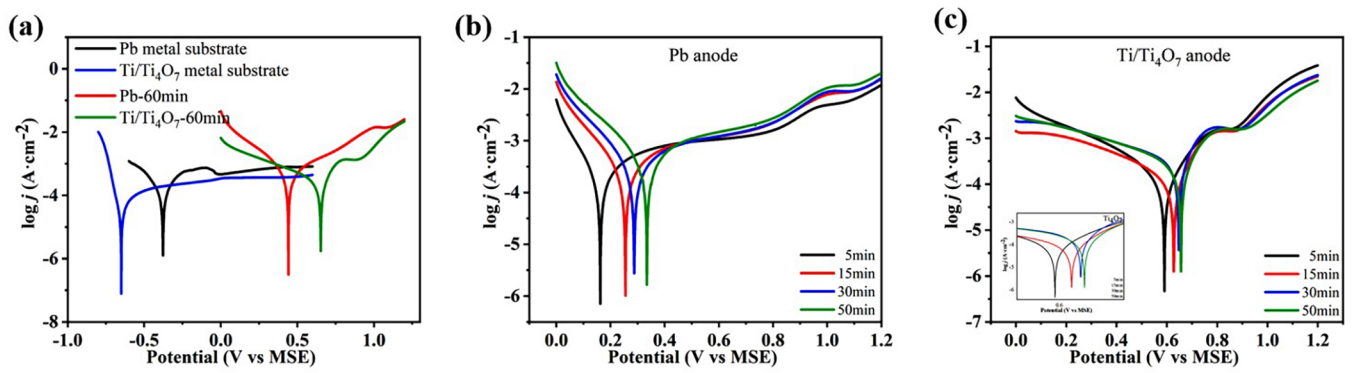

Figure 12. Tafel curves of the anode in 1 mol L^{-1} H_2SO_4: (a) anode metal matrix and polarization for 60 min, and (b, c) different polarization times of the Pb and Ti/Ti_4O_7 anodes.

reversible redox peaks. In Figure 11f, the anodic oxidation peak current density is linearly related to the square root of the potential scanning rate, indicating that the anodic reaction is controlled by the diffusion process. This is consistent with the EIS results of the above anodic reaction.

3.5. Ti/Ti_4O_7 Anode Corrosion Resistance. Corrosion potential (E_{corr}), corrosion current density (j_{corr}), and polarization resistance (R_p) were obtained by linear fitting of Tafel curves, as shown in Table 4. E_{corr} is a thermodynamic parameter to characterize the degree of difficulty of corrosion of materials in the medium. j_{corr} and R_p are kinetic parameters used to characterize the corrosion rate of the material in the medium. From Figure 12a, it can be seen that the E_{corr} of the Ti/Ti_4O_7 anode metal matrix is the smallest, which is −0.65 V, indicating that metal matrix is corroded first in acidic solution, while the E_{corr} of Pb anode is the second, which is −0.378 V. However, the j_{corr} of the Ti/Ti_4O_7 anode metal matrix is the smallest, which is 3.59×10^{-5} A cm^{-2}, and the corrosion rate in H_2SO_4 solution is the smallest. The E_{corr} of different anode metal matrixes and 60 min polarizations is as follows: Ti/Ti_4O_7-60 min > Pb-60 min > Pb metal matrix > Ti/Ti_4O_7 metal matrix. Figure 12b,c explores the effect of the MnO_2 layer formed under different anodes on the corrosion performance. Tafel tests were carried out on the anodes after galvanostatic polarization at 5, 15, 30, and 50 min. The E_{corr} of the Ti/Ti_4O_7 anode after different polarization times is higher than that of the Pb anode, indicating that the Ti/Ti_4O_7 anode has better chemical stability under the coverage of the MnO_2 layer. At the same time, j_{corr} of the Ti/Ti_4O_7 anode MnO_2 layer is smaller and the corrosion rate in the acidic system is lower. The results show that the Ti/Ti_4O_7 anode has good corrosion resistance during the electrolysis process. The reason for this is that a more stable MnO_2 layer is formed on the anode surface, which acts as a physical barrier to prevent corrosion and metal substrate oxidation.

4. CONCLUSIONS

In this study, a Ti_4O_7-coated titanium electrode was proposed as the anode for manganese electrolysis. The anode performance, anode reaction, and anode slime formation mechanism of the Ti/Ti_4O_7 anode was studied. The galvanostatic electrolysis experiment showed that the average cell voltage of the Ti/Ti_4O_7 anode was 3.752 V, which was 163 mV lower than that of the Pb anode, the current efficiency increased by 3.22%, and the energy consumption decreased by 7.82%. The anode electrochemical oscillation disappeared and the nonpower energy consumption decreased. After continuous electrolysis of 8 h, the solution anode slime was reduced 90.42% and the plate anode slime 72.80%. This remarkably reduced the energy consumption of electrolysis and the generation of anode slime. The characterization test and electrochemical analysis showed that a uniform and dense γ-MnO_2 layer quickly formed at the initial stage of electrolysis. The γ-MnO_2 has a needle-like structure and more abundant Mn (III) in the lattice, which was beneficial to lower the cell voltage and OEP. The OEP of the Ti/Ti_4O_7 anode was 324 mV lower than that of the Pb anode, and it maintained good catalytic OER activity during the electrolysis process, reversely inhibiting Mn^{2+} oxidation and reducing the formation of anode slime. Dense MnO_2 layer, lower acidity anode solution, low charge-transfer resistance, and high diffusion resistance fully inhibit the diffusion of Mn^{3+} to the solution to form solution anode slime. The application of the Ti/Ti_4O_7 anode changes the structure and morphology of the anode MnO_2 layer, significantly reduces the amount of anode slime, avoids lead pollution, and improves the current efficiency. This provides a new way to achieve the clean production and sustainable development of electrolytic manganese metal industry.

■ ASSOCIATED CONTENT

Supporting Information

The Supporting Information is available free of charge at https://pubs.acs.org/doi/10.1021/acsomega.3c05273.

Preparation method of the Ti/Ti_4O_7 anode, the XRD pattern of the Ti_4O_7 powder, anodic potential−time curves for the Ti/Ti_4O_7 anode and the Pb anode under HCC, SEM of anode slime particles under the Ti/Ti_4O_7 and Pb anodes, table of relative content ratio of Mn(III) and Mn(IV) (PDF)

■ AUTHOR INFORMATION

Corresponding Authors

Changyuan Tao − *School of Chemistry and Chemical Engineering, Chongqing University, Chongqing 400044, China; State Key Laboratory of Coal Mine Disaster Dynamics and Control, Chongqing University, Chongqing 400044, China*; Email: taocy@cqu.edu.cn

Qian Zhang − *School of Chemistry and Chemical Engineering, Chongqing University, Chongqing 400044, China*; orcid.org/0009-0004-4339-4115; Email: qianz@cqu.edu.cn

https://doi.org/10.1021/acsomega.3c05273
ACS Omega 2023, 8, 38469−38480

Authors

Haidong Zhong − *School of Chemistry and Chemical Engineering, Chongqing University, Chongqing 400044, China*

Zuohua Liu − *School of Chemistry and Chemical Engineering, Chongqing University, Chongqing 400044, China; State Key Laboratory of Coal Mine Disaster Dynamics and Control, Chongqing University, Chongqing 400044, China;* orcid.org/0000-0003-4229-0168

Jun Du − *School of Chemistry and Chemical Engineering, Chongqing University, Chongqing 400044, China;* orcid.org/0000-0003-3629-7144

Complete contact information is available at: https://pubs.acs.org/10.1021/acsomega.3c05273

Author Contributions

All the authors listed have approved the manuscript.

Notes

The authors declare no competing financial interest.

■ ACKNOWLEDGMENTS

This work was supported by the National Natural Science Foundation of China (51974045), Project No. 2022CDJQY-005 and No.2023CDJXY-047 supported by the Fundamental Research Funds for the Central Universities.

■ REFERENCES

(1) Hagelstein, K. Globally sustainable manganese metal production and use. *J. Environ. Manage.* **2009**, *90*, 3736−3740.

(2) Shu, J. C.; Liu, R. L.; Liu, Z. H.; Wu, H. P.; Chen, Y. L.; Tao, C. Y. Enhanced discharge performance of electrolytic manganese anode slime using calcination and pickling approach. *J. Electroanal. Chem.* **2017**, *806*, 15−21.

(3) Tsurtsumia, G.; Shengelia, D.; Koiava, N.; Lezhava, T.; Gogoli, D.; Beriashvili, L.; Suladze, S.; Kakhniashvili, I. Novel hydro-electrometallurgical technology for simultaneous production of manganese metal, electrolytic manganese dioxide, and manganese sulfate monohydrate. *Hydrometallurgy* **2019**, *186*, 260−268.

(4) Xie, Z. N.; Liu, Z. H.; Chang, J.; Qin, Y. B.; Tao, C. Y. Electrochemical Behaviors of MnO_2 on Lead Alloy Anode during Pulse Electrodeposition for Efficient Manganese Electrowinning. *ACS Sustainable Chem. Eng.* **2020**, *8*, 15044−15054.

(5) Ivanov, I.; Stefanov, Y.; Noncheva, Z.; Petrova, M.; Dobrev, T.; Mirkova, L.; Vermeersch, R. Insoluble anodes used in hydrometallurgy Part II. Anodic behaviour of lead and lead-alloy anodes. *Hydrometallurgy* **2000**, *57*, 125−139.

(6) Isakhani-Zakaria, M.; Allahkaram, S. R.; Ramezani-Varzaneh, H. A. Evaluation of corrosion behaviour of Pb-Co_3O_4 electrodeposited coating using EIS method. *Corros. Sci.* **2019**, *157*, 472−480.

(7) Yang, C. J. Polyoxometalate/Lead Composite Anode for Efficient Oxygen Evolution in Zinc Electrowinning. *J. Electrochem. Soc.* **2019**, *166*, E129−E136.

(8) Schmachtel, S.; Murtomaki, L.; Aromaa, J.; Lundstrom, M.; Forsen, O.; Barker, M. H. Simulation of electrochemical processes during oxygen evolution on Pb-MnO_2 composite electrodes. *Electrochim. Acta* **2017**, *245*, 512−525.

(9) Zhang, C.; Duan, N.; Jiang, L.; Xu, F.; Luo, J. Influence of Mn^{2+} ions on the corrosion mechanism of lead-based anodes and the generation of heavy metal anode slime in zinc sulfate electrolyte. *Environ. Sci. Pollut. Res.* **2018**, *25*, 11958−11969.

(10) Yu, P.; O'Keefe, T. J. Evaluation of Lead Anode Reactions in Acid Sulfate Electrolytes. *J. Electrochem. Soc.* **2002**, *149*, A558−A569.

(11) Luo, S. L.; Guo, H. J.; Lu, H.; Wang, Z. X.; Li, X. H.; Peng, W. J.; Yan, G. C.; Wang, J. X. Revealing the Reaction Mechanism of Lead Anodes in the Manganese Electrowinning Process. *ACS Sustainable Chem. Eng.* **2023**, *11*, 3517−3528.

(12) Mohammadi, M.; Alfantazi, A. The performance of Pb−MnO_2 and Pb−Ag anodes in 2 Mn(II)-containing sulphuric acid electrolyte solutions. *Hydrometallurgy* **2015**, *153*, 134−144.

(13) Lu, X.; Ning, X. A.; Lee, P. H.; Shih, K.; Wang, F.; Zeng, E. Y. Transformation of hazardous lead into lead ferrite ceramics: Crystal structures and their role in lead leaching. *J. Hazard. Mater.* **2017**, *336*, 139−145.

(14) Fan, X.; Hou, J.; Sun, D.; Xi, S.; Liu, Z.; Du, J.; Luo, J.; Tao, C. Mn-oxides catalyzed periodic current oscillation on the anode. *Electrochim. Acta* **2013**, *102*, 466−471.

(15) Fan, X.; Yang, D.; Ding, L.; Du, J.; Tao, C. Periodic current oscillation catalyzed by delta-MnO_2 nanosheets. *ChemPhysChem* **2015**, *16*, 176−180.

(16) Moats, M. S. Will lead-based anodes ever be replaced in aqueous electrowinning? *JOM* **2008**, *60*, 46−49.

(17) Liu, B.; Lyu, K.; Chen, Y.; Ma, B.; Wang, C. Energy efficient electrodeposition of metallic manganese in an anion-exchange membrane electrolysis reactor using Ti/IrO_2−RuO_2−SiO_2 anode. *J. Cleaner Prod.* **2020**, *258*, No. 120740.

(18) Luo, S. L.; Guo, H. J.; Wang, Z. X.; Li, X. H.; Wang, J. X.; Yan, G. C. The Electrochemical Performance and Reaction Mechanism of Coated Titanium Anodes for Manganese Electrowinning. *J. Electrochem. Soc.* **2019**, *166*, E502−E511.

(19) Walsh, F. C.; Wills, R. G. A. The continuing development of Magnéli phase titanium sub-oxides and Ebonex electrodes. *Electrochim. Acta* **2010**, *55*, 6342−6351.

(20) Geng, P.; Chen, G. Magnéli Ti_4O_7 modified ceramic membrane for electrically-assisted filtration with antifouling property. *J. Membr. Sci.* **2016**, *498*, 302−314.

(21) Liang, S.; Lin, H.; Yan, X.; Huang, Q. Electro-oxidation of tetracycline by a Magnéli phase Ti_4O_7 porous anode: Kinetics, products, and toxicity. *Chem. Eng. J.* **2018**, *332*, 628−636.

(22) Liu, M.; Jhulki, S.; Sun, Z.; Magasinski, A.; Hendrix, C.; Yushin, G. Atom-economic synthesis of Magnéli phase Ti_4O_7 microspheres for improved sulfur cathodes for Li−S batteries. *Nano Energy* **2021**, *79*, No. 105428.

(23) Li, X.; Zhu, A. L.; Qu, W.; Wang, H.; Hui, R.; Zhang, L.; Zhang, J. Magneli phase Ti_4O_7 electrode for oxygen reduction reaction and its implication for zinc-air rechargeable batteries. *Electrochim. Acta* **2010**, *55*, 5891−5898.

(24) Han, Z. H.; Xu, Y.; Zhou, S. G.; Zhu, P. X. Preparation and electrochemical properties of Al-based composite coating electrode with Ti_4O_7 ceramic interlayer for electrowinning of nonferrous metals. *Electrochim. Acta* **2019**, *325*, No. 134940.

(25) Ioroi, T.; Akita, T.; Asahi, M.; Yamazaki, S.-i.; Siroma, Z.; Fujiwara, N.; Yasuda, K. Platinum−titanium alloy catalysts on a Magnéli-phase titanium oxide support for improved durability in Polymer Electrolyte Fuel Cells. *J. Power Sources* **2013**, *223*, 183−189.

(26) Zhao, Z.; Zhang, J.; Yao, J.; You, S. Electrochemical removal of 4-chlorophenol in water using a porous Magnéli-phase (Ti_4O_7) electrode. *Environ. Res.* **2022**, *210*, No. 113004.

(27) Smith, J. R.; Walsh, F. C.; Clarke, R. L. Electrodes based on Magnéli phase titanium oxides: the properties and applications of Ebonex materials. *J. Appl. Electrochem.* **1998**, *28*, 1021−1033.

(28) Guo, L.; Jing, Y.; Chaplin, B. P. Development and Characterization of Ultrafiltration TiO2Magneli Phase Reactive Electrochemical Membranes. *Environ. Sci. Technol.* **2016**, *50*, 1428−1436.

(29) Tominaka, S.; Tsujimoto, Y.; Matsushita, Y.; Yamaura, K. Synthesis of nanostructured reduced titanium oxide: crystal structure transformation maintaining nanomorphology. *Angew. Chem., Int. Ed.* **2011**, *50*, 7418−7421.

(30) Zhang, C.; Jiang, L.; Xu, F.; Duan, N.; Xin, B.; Han, G.; Zhang, G.; Wen, Y. New insight into cleaner control of heavy metal anode slime from aqueous sulfate electrolytes containing Mn (II): Preliminary characterization and mechanism analysis. *J. Cleaner Prod.* **2018**, *177*, 276−283.

(31) Lu, J. M.; Dreisinger, D.; Gluck, T. Manganese electrodeposition - A literature review. *Hydrometallurgy* **2014**, *141*, 105−116.

(32) Luo, S. L.; Guo, H. J.; Zhang, S. K.; Wang, Z. X.; Li, X. H.; Peng, W. J.; Wang, J. X.; Yan, G. C. Efficient production of metal manganese achieved by cylindrical and rotary electrode. *J. Cleaner Prod.* **2021**, *326*, No. 129266.
(33) Xie, Z.; Liu, Z.; Tao, C.; Li, C.; Chang, J. Production of electrolytic manganese metal using a new hyperchaotic circuit system. *J. Mater. Res. Technol.* **2022**, *18*, 4804−4815.
(34) Moazzen, E.; Timofeeva, E. V.; Segre, C. U. Controlled synthesis of MnO_2 nanoparticles for aqueous battery cathodes: polymorphism−capacity correlation. *J. Mater. Sci.* **2017**, *52*, 8107−8118.
(35) Ye, W. Q.; Xu, F. Y.; Jiang, L. H.; Duan, N.; Li, J. H.; Zhang, F. L.; Zhang, G.; Chen, L. J. A novel functional lead-based anode for efficient lead dissolution inhibition and slime generation reduction in zinc electrowinning. *J. Cleaner Prod.* **2021**, *284*, No. 124767.
(36) Tang, B.; Yang, F.; Chen, C.; Shi, C.; Deng, W.; Li, J.; Jiang, L. A novel lead-based pseudo dimensional stable anode toward efficient and clean extraction of metallic manganese. *J. Cleaner Prod.* **2023**, *386*, No. 135806.
(37) Huang, X.; Zhao, G.; Chang, Y.; Wang, G.; Irvine, J. T. S. Nanocrystalline $CeO_{2-\delta}$ coated β-MnO_2 nanorods with enhanced oxygen transfer property. *Appl. Surf. Sci.* **2018**, *440*, 20−28.
(38) Zhu, Y. P.; Xia, C.; Lei, Y. J.; Singh, N.; Schwingenschlogl, U.; Alshareef, H. N. Solubility contrast strategy for enhancing intercalation pseudocapacitance in layered MnO_2 electrodes. *Nano Energy* **2019**, *56*, 357−364.
(39) Cakici, M.; Reddy, K. R.; Alonso-Marroquin, F. Advanced electrochemical energy storage supercapacitors based on the flexible carbon fiber fabric-coated with uniform coral-like MnO_2 structured electrodes. *Chem. Eng. J.* **2017**, *309*, 151−158.
(40) Ilton, E. S.; Post, J. E.; Heaney, P. J.; Ling, F. T.; Kerisit, S. N. XPS determination of Mn oxidation states in Mn (hydr)oxides. *Appl. Surf. Sci.* **2016**, *366*, 475−485.
(41) Gupta, P. K.; Bhandari, A.; Saha, S.; Bhattacharya, J.; Pala, R. G. S. Modulating Oxygen Evolution Reactivity in MnO_2 through Polymorphic Engineering. *J. Phys. Chem. C* **2019**, *123*, 22345−22357.
(42) Morgan Chan, Z.; Kitchaev, D. A.; Nelson Weker, J.; Schnedermann, C.; Lim, K.; Ceder, G.; Tumas, W.; Toney, M. F.; Nocera, D. G. Electrochemical trapping of metastable Mn^{3+} ions for activation of MnO_2 oxygen evolution catalysts. *Proc. Natl. Acad. Sci. U.S.A.* **2018**, *115*, E5261−E5268.
(43) Clarke, C. J.; Browning, G. J.; Donne, S. W. An RDE and RRDE study into the electrodeposition of manganese dioxide. *Electrochim. Acta* **2006**, *51*, 5773−5784.
(44) Lai, Y.; Li, Y.; Jiang, L.; Xu, W.; Lv, X.; Li, J.; Liu, Y. Electrochemical behaviors of co-deposited Pb/Pb−MnO_2 composite anode in sulfuric acid solution − Tafel and EIS investigations. *J. Electroanal. Chem.* **2012**, *671*, 16−23.
(45) Mohammadi, M.; Mohammadi, F.; Alfantazi, A. Electrochemical Reactions on Metal-Matrix Composite Anodes for Metal Electrowinning. *J. Electrochem. Soc.* **2013**, *160*, E35−E43.
(46) Pajkossy, T.; Jurczakowski, R. Electrochemical impedance spectroscopy in interfacial studies. *Curr. Opin. Electrochem.* **2017**, *1*, 53−58.
(47) Pan, M.; Zhang, Y.; Shan, C.; Zhang, X.; Gao, G.; Pan, B. Flat Graphene-Enhanced Electron Transfer Involved in Redox Reactions. *Environ. Sci. Technol.* **2017**, *51*, 8597−8605.
(48) Barbero, G.; Lelidis, I. Analysis of Warburg's impedance and its equivalent electric circuits. *Phys. Chem. Chem. Phys.* **2017**, *19*, 24934−24944.
(49) Zhu, K.; Neale, N. R.; Miedaner, A.; Frank, A. J. Enhanced Charge-Collection Efficiencies and Light Scattering in Dye-Sensitized Solar Cells Using Oriented TiO_2 Nanotubes Arrays. *Nano Lett.* **2007**, *7*, 69−74.
(50) Macak, J. M.; Zlamal, M.; Krysa, J.; Schmuki, P. Self-organized TiO_2 nanotube layers as highly efficient photocatalysts. *Small* **2007**, *3*, 300−304.
(51) Harriman, K.; Gavaghan, D. J.; Houston, P.; SUli, E. Adaptative finite element simulation of currents at microelectrodes to a guaranteed accuracy. First-order EC' mechanism at inlaid and recessed discs. *Electrochem. Commun.* **2000**, *2*, 163−170.

https://doi.org/10.1021/acsomega.3c05273
ACS Omega 2023, 8, 38469−38480